Dual wavelength *Q*-switched cascade laser

Jianfeng Li,[1,2,*] Tomonori Hu,[1] and Stuart D. Jackson[1]

[1]*Institute of Photonics and Optical Science (IPOS) and Centre for Ultrahigh-bandwidth Devices for Optical Systems (CUDOS), School of Physics, University of Sydney, Camperdown 2006, Australia*

[2]*State Key Laboratory of Electronic Thin Films and Integrated Devices, School of Optoelectronic Information, University of Electronic Science and Technology of China, Chengdu 610054, China*

**Corresponding author: lijianfeng@uestc.edu.cn*

Received March 6, 2012; revised April 12, 2012; accepted April 12, 2012;
posted April 13, 2012 (Doc. ID 164239); published June 4, 2012

A diode-cladding-pumped dual wavelength *Q*-switched Ho^{3+}-doped fluoride cascade fiber laser operating in the mid-infrared is demonstrated. Stable pulse trains from the $^5I_6 \rightarrow {}^5I_7$ and $^5I_7 \rightarrow {}^5I_8$ laser transitions were produced, and the μs-level time delay between the pulses from each transition was dependent on the pump power. At maximum pump power and at an acousto-optic modulator repetition rate of 25 kHz, the $^5I_6 \rightarrow {}^5I_7$ transition pulse operated at 3.005 μm, a pulse energy of 29 μJ, and a pulse width of 380 ns; the $^5I_7 \rightarrow {}^5I_8$ transition pulse correspondingly produced 7 μJ pulse energy and 260 ns pulse width at 2.074 μm. To the best of our knowledge, this is the first demonstration of a *Q*-switched fiber laser operating beyond 3 μm. © 2012 Optical Society of America

OCIS codes: 140.3510, 140.3480.

Mid-infrared (mid-IR) fluoride glass fiber lasers have a number of potential applications in defense, medicine, and chemical sensing. Compared to cw fiber lasers, pulsed fiber lasers are desirable because they offer high peak power that can be used directly or shifted to other wavelengths using nonlinear frequency conversion. A number of fluoride glass pulsed fiber lasers have been reported based on Er^{3+}-doped and Er^{3+}–Pr^{3+} co-doped fluoride fibers [1–6]. The recent report of a gain-switched 2.8 μm Er^{3+}-doped ZBLAN fiber laser with pulse duration of 300 ns and average power of 2 W at 100 kHz repetition rate [5] and actively *Q*-switched 2.8 μm Er^{3+}-doped ZBLAN fiber laser with 90 ns duration and 12 W average power [6] marked the beginning of the development of pulsed 3 μm class fluoride fiber lasers with high average power and short pulse width. Extending the emission wavelength from pulsed fiber lasers is desirable as a result of their potential role as pump sources in mid-IR photonics and nonlinear optics.

Cascade lasing of both the $^5I_6 \rightarrow {}^5I_7$ and $^5I_7 \rightarrow {}^5I_8$ laser transitions of a Ho^{3+}-doped fluoride fiber laser has been demonstrated in cw operation [7,8]. A recent report of a Watt-level diode-cladding-pumped Ho^{3+}-doped fluoride cascade fiber laser free running at 3.002 μm [9] demonstrated that Ho^{3+}-dopedfluoride glass fiber lasers can extend the emission wavelength into the mid-IR. Moreover, the cascade lasing on both the $^5I_6 \rightarrow {}^5I_7$ and the $^5I_7 \rightarrow {}^5I_8$ laser transitions is a straight forward process not reliant on strong cavity resonances and offers the opportunity for all infrared emission with little visible light generation owing to comparatively reduced levels of pump excited state absorption. Cascade lasing also provides the opportunity to obtain pulses at both 3 μm and 2 μm in a simple actively *Q*-switched arrangement.

In this letter, we demonstrate a *Q*-switched cascade fluoride laser that produced pulses at 3.005 μm and 2.074 μm simultaneously using a TeO_2 acousto-optic modulator (AOM). The 3 μm and 2 μm pulses have a μs-level time delay and operate at the same repetition rate within a pump power dependent repetition rate range that provides stable pulses.

The experimental arrangement for the *Q*-switched cascade Ho^{3+}-doped ZBLAN fiber laser is shown in Fig. 1. The Ho^{3+}-doped double clad fiber (FiberLabs, Japan) was identical to the fiber used in our previous free running experiment [9] and had a *D*-shaped pump core with a diameter of 125 μm across the circular cross-section and a numerical aperture (NA) of 0.50. The fiber had a 10 μm core diameter with an NA of 0.16. The Ho^{3+} concentration of the fiber was chosen to be 1.2 mol% to reduce energy transfer processes between Ho^{3+} ions; this concentration has not been identified as optimal. The selected fiber length of 12.0 m was longer than that used in our previous experiment, providing higher pump absorption efficiency and longer emission wavelength. The absorption coefficient of the fiber and the launch efficiency were measured to be 0.28 m^{-1} and 84%, respectively, using cutback measurements. Each end of the fiber was held in place by commercial fiber *V*-groove holders and the remaining fiber was coiled onto an aluminium spool with a bend radius of 15 cm. An active cooling system was not necessary owing to the small absorption coefficient.

Commercially available high power 1.15 μm diode lasers (Eagleyard Photonics, Berlin) were used to pump each end of the fiber after polarization multiplexing

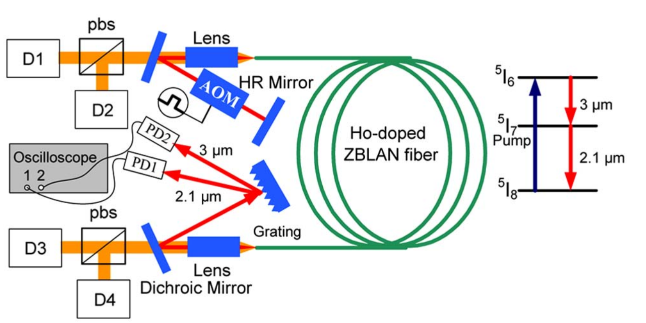

Fig. 1. (Color online) Schematic of the experiment setup. D1–D4 represents the pump diodes, pbsrepresents the polarizing beam splitter, and PD1 and PD2 represent the photo detectors. Included is a simplified energy level diagram of the Ho^{3+}ion showing the pump and cascade laser transitions.

and focusing using two antireflection-coated ZnSe objective lenses (Innovation Photonics, LFO-5-6-3.0 μm, 0.25 NA) with focal lengths of 6 mm which collimated the $^5I_6 \rightarrow {}^5I_7$ and $^5I_7 \rightarrow {}^5I_8$ laser transition outputs emitted from the fiber core. The measured transmission for 1.15 μm and 2 μm emissions were 80% and 92%, respectively. Two highly pump-transmitting dichroic mirrors with reflectivity of 60% between 2.0 μm and 2.1 μm and >98% between 2.5 μm and 3.2 μm were each positioned between the polarizing beam splitter and focusing lens at angle of 15° with respect to the pump beam. One dichroic mirror was used to steer the emission onto the TeO_2 AOM that had a rise time of 115 ns, and the other mirror was used to direct the fiber laser output. The AOM with a transmission of 89% at 2 μm and 86% at 3 μm was placed into the extended part of the cavity in a zero-order arrangement and was driven by a pulsed RF source. The measured diffraction efficiencies of this AOM were 80% and 83% for emissions at 2 μm and 3 μm, respectively. To avoid parasitic lasing, the fiber end closest to the AOM was cleaved at an angle of ~8°.

For the measurements of the laser output, a gold-coated plane ruled grating (300 lines per mm, blaze wavelength $\lambda_B = 2$ μm, blaze angle $\theta_B = 17.5°$) was used to separate the two transitions of the cascade. Two InAs photodiodes with a response time of approximately 10 ns, connected to two channels of a 100 MHz two-channel digital storage oscilloscope (Tektronix TDS1012), were used to measure the pulse train and pulse characteristics. An optical spectrum analyzer (Yokogawa AQ6375, Japan) was used to measure the laser spectrum at 2.1 μm. The spectrum at 3 μm was measured using a calibrated monochromator (with 0.3 nm resolution) that employed a thermoelectrically cooled InAs photodiode.

By adjusting the switching rate of the AOM, stable pulse trains from the $^5I_6 \rightarrow {}^5I_7$ and $^5I_7 \rightarrow {}^5I_8$ laser transitions could be produced. Figure 2 shows the output trains and temporal pulse shape at a repetition rate of 25 kHz for the maximum launched pump power of 7.4 W. For $^5I_6 \rightarrow {}^5I_7$ transition pulse, an average power of 745 mW with a threshold of 310 mW was produced at a slope efficiency of 12.1%, which is similar to the 762 mW produced in free running mode when the AOM was switched off. The measured pulse width (FWHM) of 380 ns is much longer than that reported in [6]; a result of the longer laser cavity and lower pump rate. The average pulse energy and peak power were calculated to be 30 μJ and 78 W, respectively. After a time delay of ~1.7 μs, a stable pulse from $^5I_7 \rightarrow {}^5I_8$ transition was measured. The delay relates to the fact that the $^5I_7 \rightarrow {}^5I_8$ transition relies on the $^5I_6 \rightarrow {}^5I_7$ transition pulse to create a population in the $^5I_7$ level. A maximum average power of 175 mW with a threshold pump power of 3.2 W was produced at the slope efficiency of 4.5%. The pulse had 260 ns duration, an estimated energy of 7.5 μJ, and a peak power of 29 W. The low slope efficiency compared to calculations [10] and free-running Ho^{3+}, Pr^{3+}-doped fluoride fiber lasers [11] is an issue that may relate to Ho^{3+} ion clustering, the fabrication process, or the glass composition; we are currently carrying out an investigation to identify the problem. The pulse-to-pulse amplitude stability for both $^5I_6 \rightarrow {}^5I_7$ and $^5I_7 \rightarrow {}^5I_8$ transitions was approximately ±5%. The right inset to Fig. 2 shows the time delay between the $^5I_6 \rightarrow {}^5I_7$ and $^5I_7 \rightarrow {}^5I_8$ transition pulses as a function of launched pump power. It is observed that the time delay decreased quickly with launched pump power as a result of the shorter build up time of the population in the $^5I_7$ level and the increasing rate of ground state absorption (GSA).

Figure 3 shows the optical spectrum of the output for free running and pulsed operation at maximum launched pump power. The free running $^5I_6 \rightarrow {}^5I_7$ transition operatesat a center wavelength of 3.005 μm and bandwidth of 4 nm; under Q-switched conditions, the bandwidth broadens to 10 nm because more Stark levels are involved in the laser emission as a result of the transient nature of the Q-switching process itself. The free running $^5I_7 \rightarrow {}^5I_8$ transition operates at a center wavelength of 2.074 μm and bandwidth of 2 nm which broadens to 5 nm. Note that the emission wavelength of the $^5I_6 \rightarrow {}^5I_7$ transition is now longer than the measurements made in [9] which involved a shorter fiber length of 10 m. The longer fiber length in the current demonstration forces a higher threshold for the $^5I_7 \rightarrow {}^5I_8$ transition

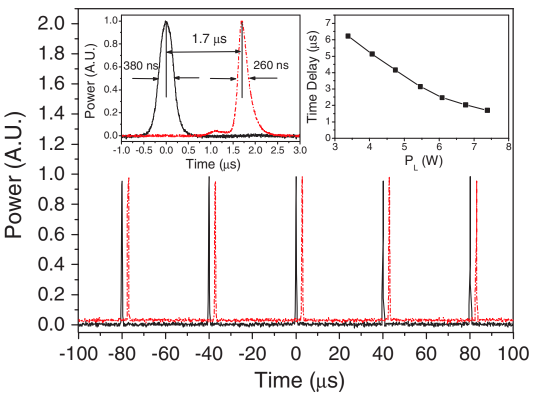

Fig. 2. (Color online) Measured output pulse trains for the $^5I_6 \rightarrow {}^5I_7$ and $^5I_7 \rightarrow {}^5I_8$ transitions at the repetition rate of 25 kHz for the maximum launched pump power of 7.4 W. The left inset shows the temporal pulse waveform for $^5I_6 \rightarrow {}^5I_7$ (solid line) and $^5I_7 \rightarrow {}^5I_8$ (dashed line) transitions. The right inset shows the time delay between thetwo transitions as a function of launched pump power, P_L.

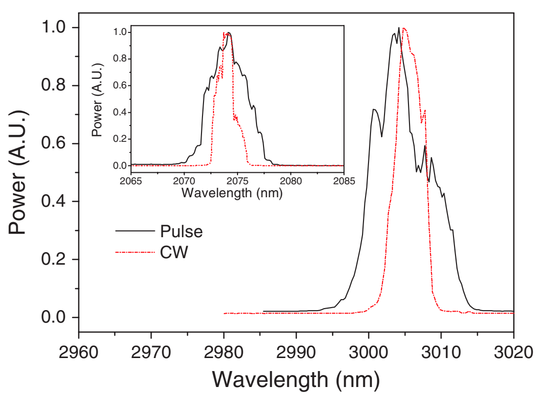

Fig. 3. (Color online) Measured spectrum of the $^5I_6 \rightarrow {}^5I_7$ laser transition for CW and pulsed operation at maximum pump power. The inset shows the measured spectrum for the $^5I_7 \rightarrow {}^5I_8$ laser transition for CW and pulse operation at maximum pump power.

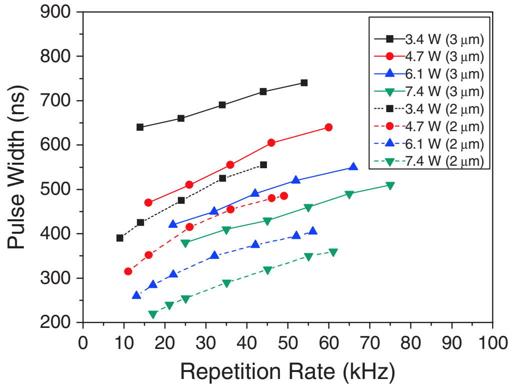

Fig. 4. (Color online) Measured pulse width of the 3 μm and 2.1 μm transitions as a function of repetition frequency at four different launched pump powers.

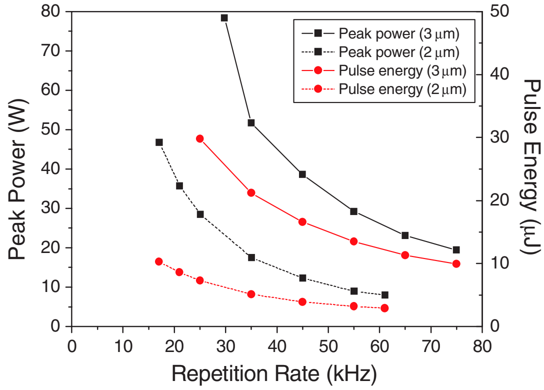

Fig. 5. (Color online) Measured pulse peak power and pulse energy of the $^5I_6 \rightarrow {}^5I_7$ and $^5I_7 \rightarrow {}^5I_8$ laser transitions as a function of the repetition rate at a launched pump power of 7.4 W.

which increases the population in the $^5I_7$ manifold and the terminating Stark level for the $^5I_6 \rightarrow {}^5I_7$ transition is now higher up the $^5I_7$ manifold.

Figure 4 shows the pulse widths for the 3 μm and 2.1 μm transitions as a function of repetition rate and launched pump power. The stable pulse range for both 3 μm and 2.1 μm transitions shifted to larger repetition rate with increased launched pump power. At maximum pump power, the stable pulse repetition rate range for the 3 μm and 2.1 μm transitions was 25 kHz to 75 kHz and 17 kHz to 61 kHz, respectively. Multiple pulsing occurred outside these ranges. The pulsed 2.1 μm and 3 μm transitions operated at the same repetition rate between 25 kHz and 61 kHz at maximum launched pump power. The pulse width of each 3 μm and 2.1 μm transition decreased with increased launched pump power and increased with increased repetition rate, as expected with actively Q-switched lasers. The narrowest pulse width of 380 ns for the 3 μm pulse and 220 ns for the 2.1 μm pulse were obtained at 25 kHz and 17 kHz, respectively.

The peak power and pulse energy of the 3 μm and 2.1 μm pulses as a function of the repetition rate at the maximum launched pump power of 7.4 W are shown in Fig. 5. The average power for both transitions remained essentially unchanged across the range of the repetition rates allowing stable pulse formation. The pulse energy was inversely proportional to the repetition rate; the pulse energy decreased to 10 μJ at 75 kHz for 3 μm emission and decreased to 3.6 μJ at 47 kHz for 2.1 μm emission. The peak power decreased more significantly with the repetition rate than the pulse energy because of the concomitant increasing pulse width.

The demonstrated center emission wavelength of 3.005 μm, peak power of 78 W and pulse width of 380 ns are encouraging results from the first Q-switched fiber laser operating beyond 3 μm.The decreasing time delay between the 3 μm and 2.1 μm pulses with increased launched pump power suggests that the delay between pulses could be < 1 μs at higher launched pump power. The angle cleave on the intracavity fiber end was most likely instrumental in achieving stable pulse formation over a broad range of repetition rates.

In summary, we have demonstrated what we believe to be the first Q-switched cascade laser involving two electronic transitions operating simultaneously. A maximum peak power of 79 W and 49 W was obtained from the 3.005 μm and 2.074 μm transition, respectively. Further improvement in the peak power level is expected with increased pumping and tuning the Q-switched cascade laser is expected to extend the emission wavelength further into the mid-IR.

The authors acknowledge financial support from the Australian Research Council through the Discovery Projects and Centre of Excellence funding schemes. SJ acknowledges support from a Queen Elizabeth II Fellowship. This work was also supported by National Nature Science Foundation of China (Grant No. 61107037 and 60925019), China Postdoctoral Science Special Foundation (Grant No. 201003693), and the Fundamental Research Funds for the Central Universities (Grant No. ZYGX2009J053). The Centre for Ultrahigh bandwidth Devices for Optical Systems (CUDOS) is an ARC Centre of Excellence.

References

1. C. Frerichs and T. Tauermann, Electron. Lett. **30**, 706 (1994).
2. C. Frerichs and U. B. Unrau, Opt. Fiber Technol. **2**, 358 (1996).
3. N. Libatique, J. Tafoya, S. H. Feng, D. Mirell, and R. Jain, in *Advanced Solid State Lasers* OSA Technical Digest Series (Optical Society of America, 2000), paper MD2.
4. T. Segi, K. Shima, T. Sakai, and H. Hosoya, in *Conference on Lasers and Electro-Optics (CLEO)*, Technical Digest (Optical Society of America, 2004), paper CThZ5.
5. M. Gorjan, R. Petkovšek, M. Marinček, and M. Čopič, Opt. Lett. **36**, 1923 (2011).
6. S. Tokita, M. Murakami, S. Shimizu, M. Hashida, and S. Sakabe, Opt. Lett. **36**, 2812 (2011).
7. T. Sumiyoshi, H. Sekita, T. Arai, S. Sato, M. Ishihara, and M. Kikuchi, IEEE J. Select. Topics Quantum Electron. **5**, 936 (1999).
8. T. Sumiyoshi and H. Sekita, Opt. Lett. **23**, 1837 (1998).
9. J. Li, D. D. Hudson, and S. D. Jackson, Opt. Lett. **36**, 3642 (2011).
10. J. Li, L. Gomes, and S. D. Jackson, IEEE J. Quantum Electron. **48**, 596 (2012).
11. S. D. Jackson, Opt. Lett. **34**, 2327 (2009).